

Refined nonlinear fractional derivative model of vehicle-track coupling dynamics

Yang, Fan; Zhang, Pan; Wang, Yuan; Wei, Kai; Dong, Liwei; Wang, Ping

DOI

[10.1016/j.ijnonlinmec.2023.104444](https://doi.org/10.1016/j.ijnonlinmec.2023.104444)

Publication date

2023

Document Version

Final published version

Published in

International Journal of Non-Linear Mechanics

Citation (APA)

Yang, F., Zhang, P., Wang, Y., Wei, K., Dong, L., & Wang, P. (2023). Refined nonlinear fractional derivative model of vehicle-track coupling dynamics. *International Journal of Non-Linear Mechanics*, 154, Article 104444. <https://doi.org/10.1016/j.ijnonlinmec.2023.104444>

Important note

To cite this publication, please use the final published version (if applicable).
Please check the document version above.

Copyright

Other than for strictly personal use, it is not permitted to download, forward or distribute the text or part of it, without the consent of the author(s) and/or copyright holder(s), unless the work is under an open content license such as Creative Commons.

Takedown policy

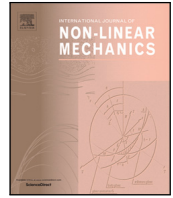
Please contact us and provide details if you believe this document breaches copyrights.
We will remove access to the work immediately and investigate your claim.

Green Open Access added to TU Delft Institutional Repository

'You share, we take care!' - Taverne project

<https://www.openaccess.nl/en/you-share-we-take-care>

Otherwise as indicated in the copyright section: the publisher is the copyright holder of this work and the author uses the Dutch legislation to make this work public.



Refined nonlinear fractional derivative model of vehicle-track coupling dynamics

Fan Yang^{a,b,1}, Pan Zhang^{c,1}, Yuan Wang^d, Kai Wei^{e,f,*}, Liwei Dong^b, Ping Wang^{e,f,*}

^a Department of Orthopaedics, Shanghai Key Laboratory for Prevention and Treatment of Bone and Joint Diseases, Shanghai Institute of Traumatology and Orthopaedics, Ruijin Hospital, Shanghai Jiao Tong University School of Medicine, Shanghai, 200025, China

^b Institute of Rail Transit, Tongji University, Shanghai, 201804, China

^c Delft University of Technology, Section of Railway Engineering, Stevinweg 1, 2628 CN, Delft, The Netherlands

^d School of System Design and Intelligent Manufacturing, Southern University of Science and Technology, Shenzhen, China

^e School of Civil Engineering, Southwest Jiaotong University, Chengdu 610031, China

^f Key Laboratory of High-speed Railway Engineering, Ministry of Education, Chengdu 610031, China

ARTICLE INFO

Keywords:

Vehicle-track coupled dynamics
Nonlinear fractional derivative model
Finite element method
High frequency
Elastic wheelset

ABSTRACT

The coupled vehicle-track system (CVTS) dynamics have been extensively investigated for decades. However, the calculation accuracy of prevailing vehicle-track coupling models needs to be improved in the high frequency range due to the inappropriate model simplification and neglect of material nonlinearity. In this study, we propose a refined numerical model of the CVTS that considers the nonlinear properties of the railpads and primary suspension using the fraction derivative Zener model. Furthermore, we more realistically simulate the wheelset, rail and railpad configuration with the elastic axle, solid finite element and surface-support models, respectively, and improve the computation efficiency by employing the mode superposition method. The results demonstrate that the refined CVTS model is more accurate than the classical model in simulating vehicle-track coupling dynamics above 2 kHz. In particular, there are significant differences in the dynamic response of the elastic wheelset model compared to the rigid model over a broad frequency range, with an 11% difference in the bogie acceleration response at the first dominant frequency. When the railpads are modeled using the surface-support model, the rail acceleration differences exceed 41% near 1 kHz and 44% near 2650 Hz, compared to the point-support model. Additionally, the rail response at various locations across the rail cross section can be calculated using the finite element method in this refined model. Overall, the proposed CVTS model provides high accuracy and efficiency for random vibration analysis, especially in the high frequency domain.

1. Introduction

With the rapid development of high-speed railway networks, the cumulative structural damage of ballastless tracks caused by high-frequency wheel-rail interactions has increased significantly. Such damage includes rail corrugation, irregular wheel profiles, spring bar fractures, and track plate cracks [1–5]. The high-frequency vibration characteristics of wheelsets and rails are primarily determined by the track irregularity spectrum, vehicle speed, and various nonlinear dynamic parameters dependent on the frequency and amplitude of external excitation, including viscoelastic polymer materials used as the primary suspensions of the vehicle and railpads [6,7]. To accurately predict, analyze, and control the high-frequency random vibration of the coupled vehicle-track system (CVTS), numerous theoretical studies [8] have focused on the elastic modeling of wheelsets

and rails, high-frequency wheel-rail interaction, and nonlinear dynamic characteristics of polymeric materials in the vehicle and track systems.

The dynamic behavior of rails and vibration analysis of the coupled vehicle-track system (CVTS) are typically described using the Timoshenko beam element which considers shear deformation and rotational bending effects [9–11]. With the advancement of computer capacity, the finite element method (FEM) has been increasingly employed to study the wheel-rail impact response induced by such as rail joints [12], corrugation [13], wheel flats [14] and wheel polygonization [15]. Wei et al. [16,17] developed a high-frequency vibration model for the CVTS using a solid finite element model of wheelsets, and investigated the high-frequency vibration response of wheel-rail interactions subjected to track irregularities. Casas et al. [18] established a three-dimensional (3D) track model based on the moving

* Corresponding author at: 999 Xian'an Road, Pidu District, Chengdu, Sichuan Province, 610031, China.

E-mail addresses: weimike@home.swjtu.edu.cn (K. Wei), wping@home.swjtu.edu.cn (P. Wang).

¹ These authors contributed equally to this work.

element method to replace the earlier Timoshenko beam model, and used this model to obtain simulation results under various excitations. Torstensson et al. [19], and Sladkowski et al. [20] developed an elastic FEM of the CVTS to analyze the high-frequency vibration response of the wheelsets and track. Knothe et al. [21] conducted a comparison between the beam model and the 2D plate model of rails to analyze their dynamic response at high frequencies. They proposed a new model based on the FEM to improve the accuracy of the analysis. Lei et al. [22] developed an approach with FE to investigate the dynamic response of the vehicle-slab track coupling system. Baeza et al. [23] proposed three formulas for railway structure dynamics in the high frequency domain, based on an Eulerian approach to model rotating flexible wheelset. Xu et al. [24] proposed a 3D model for the vehicle-track interactions based on wheel-rail coupling models and energy-variational principle. Besides, the 3D FE approach was applied to simulate the high-frequency vibrations and wheel-rail frictional rolling contact of the wheel-track system [25–27]. The previous researches have focused on exploring the high-frequency vibration of wheel-rail coupling through the development of elastic finite element models for either the vehicle or the track. Nevertheless, these models still fall short in accurately predicting the response of the coupled system in the high frequency domain. This is largely due to the lack of consideration for the material nonlinearity of elastic rubber components, particularly the primary suspension and railpads of the vehicle-track system.

In the vehicle-track system, rubber materials can serve as elastic elements in the suspension system and as railpads in the fastening systems. With increasing train speeds, the mechanical behavior of these rubber components can have a significant impact on the dynamic interaction between the wheels and rails. The dynamic properties of rubber materials, including elasticity and damping, exhibit strong dependence on frequency and amplitude owing to their nonlinear viscoelastic nature [6]. An effective way to describe these nonlinear properties of the rubber materials is to use a constitutive relation containing fractional derivatives (FD) [28,29]. Pritz et al. [30,31] first implemented FD models to represent the nonlinear properties of polymeric damping materials. Schmidt et al. [32] applied the FD scheme to create FE formulations for constitutive relations of viscoelastic materials. Coulomb forces can be incorporated into the frictional behavior model of carbon black filled rubber [33]. Berg et al. gave a developed a smooth friction model based on Coulomb force that is dependent on deformation and elastic force [34,35]. Fenander et al. [36,37] proposed a railway track model that incorporates a FD model of railpads and examined the differences in track vibration characteristics between their model and the conventional model. Sjöberg et al. [38,39] developed a nonlinear FD model for the primary suspension, and its superiority over the traditional Kelvin-Voigt model was validated. Similarly, Zhu et al. [40] proposed a frequency-dependent model for railpads and conducted an investigation into the nonlinear dynamics of the slab track system. Zhang et al. [41] also developed a nonlinear model of the primary suspension of a freight vehicle with FD theory and Berg's friction model. Yang et al. [42,43] investigated the frequency-dependent dynamic behavior of the rubber springs in the CVTS using the FD Zener model, which provides a better expression of the frequency dependence compared to traditional models. They also applied this model to study the random vibration of the CVTS in extreme cold weather and proposed optimal energy harvesting approaches using a rail-bore generator [43–45]. The above mentioned studies have high computational accuracy in the first wheel-track resonance frequency band. However, in the high-frequency range, further improvement is needed due to inadequate model simplification, such as treating the wheelset as a rigid body and the rail as a beam.

Overall, the random vibration model of the CVTS in the high frequency domain can be improved in two ways, by considering the nonlinear properties of the viscoelastic rubber materials, and by employing the elastic models of the wheelset and track system. However, the existing studies rarely simultaneously take into account these two aspects.

In this paper, an advanced nonlinear dynamic model of the CVTS was developed by comprehensively including the flexible wheelset model, the solid element rail model, and the nonlinear FD Zener model of both primary suspensions and railpads. Besides, the computation efficiency of this model is improved by employing the mode superposition method. Therefore, the proposed model can achieve both high solution accuracy and computation efficiency for characterizing the random dynamic behaviors of the CVTS in a broad frequency domain.

2. Methodology

In this section, we first introduce the nonlinear FD Zener model in a single degree of freedom system (Section 2.1), then applied it in the refined nonlinear model of the CVTS (Section 2.2), and finally solved its steady state vibration response in the frequency range (Section 2.3).

2.1. The nonlinear FD Zener model in a single degree of freedom system

Rubber materials display nonlinear dynamic behavior that can be effectively characterized by employing the FD model and Coulomb friction model, as reported in the previous study [38]. Fig. 1 illustrates the physical and mechanical models of the railpad. In view of the frequency and amplitude dependence of the railpad, the force acting between the mass block and base can be divided into two components: the viscoelastic force denoted as F_α , and the friction force represented as F_f .

The force-displacement relationship for the FD Zener model can be represented in a general form as follows [42].

$$F_\alpha(t) + a_\alpha D^\alpha F_\alpha(t) = b_\alpha x(t) + c_\alpha D^\alpha x(t) \quad (1)$$

where, F_α is the FD viscoelastic force; $x(t)$ is displacement; a_α , b_α , c_α , and α are the model coefficients of railpads; D^α is the FD operator.

The friction force F_f , exhibiting vibration amplitude dependence, is a function of both displacement and reference state. The friction force can be obtained by nonlinear Berg's friction model as follows [34].

$$\begin{cases} F_f = F_{fs}, & x = x_s \\ F_f = F_{fs} + \frac{x - x_s}{x_2(1 - \mu) + (x - x_s)} (F_{fmax} - F_{fs}), & x > x_s \\ F_f = F_{fs} + \frac{x - x_s}{x_2(1 + \mu) - (x - x_s)} (F_{fmax} - F_{fs}), & x < x_s \end{cases} \quad (2)$$

where, $\mu = F_{fs}/F_{fmax}$. The friction force, F_f , in the present model depends, like the elastic force, on the displacement x over the element. x_s and F_{fs} indicate a reference state of friction force versus displacement. F_{fmax} and x_2 represent the maximum friction force and displacement when F_f is equal to $F_{fmax}/2$, respectively.

By employing the nonlinear constitutive model of the rubber materials, the dynamic response of the rigid mass m under a harmonic excitation can be expressed as follows.

$$m\ddot{x}(t) + F_\alpha(t) + F_f(t) = F \cos(\omega t) \quad (3)$$

2.2. The refined nonlinear FD Zener model of the CVTS

2.2.1. The refined rigid-elastic model of the vehicle

The nonlinear FD Zener model of the spatial vehicle structure consists of the car body, bogies, wheelsets, primary and secondary suspensions. The primary suspension system was expressed by the nonlinear FD Zener model, while the secondary suspension was regarded as a classic KV model (see Fig. 2a~c). As the study focuses on the vertical vibration of the spatial CVTS, the vehicle system (except for 4 wheelsets) can be considered as a classic multi-rigid body system with 9 degrees of freedom (DOFs) of the car body and bogies. The 9 DOFs include: (1) vertical displacement of the car body, front bogie and rear bogie (Z_c , Z_{t1} , Z_{t2}); (2) pitch angle of the car body, front bogie and

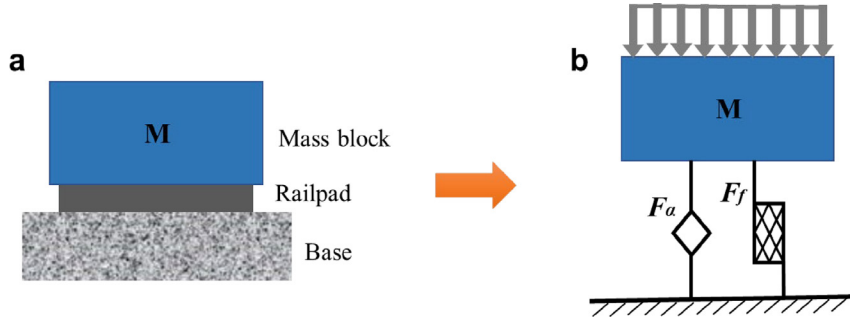


Fig. 1. Nonlinear FD Zener model of an SDOF system. (a) physical model; (b) mechanical model.

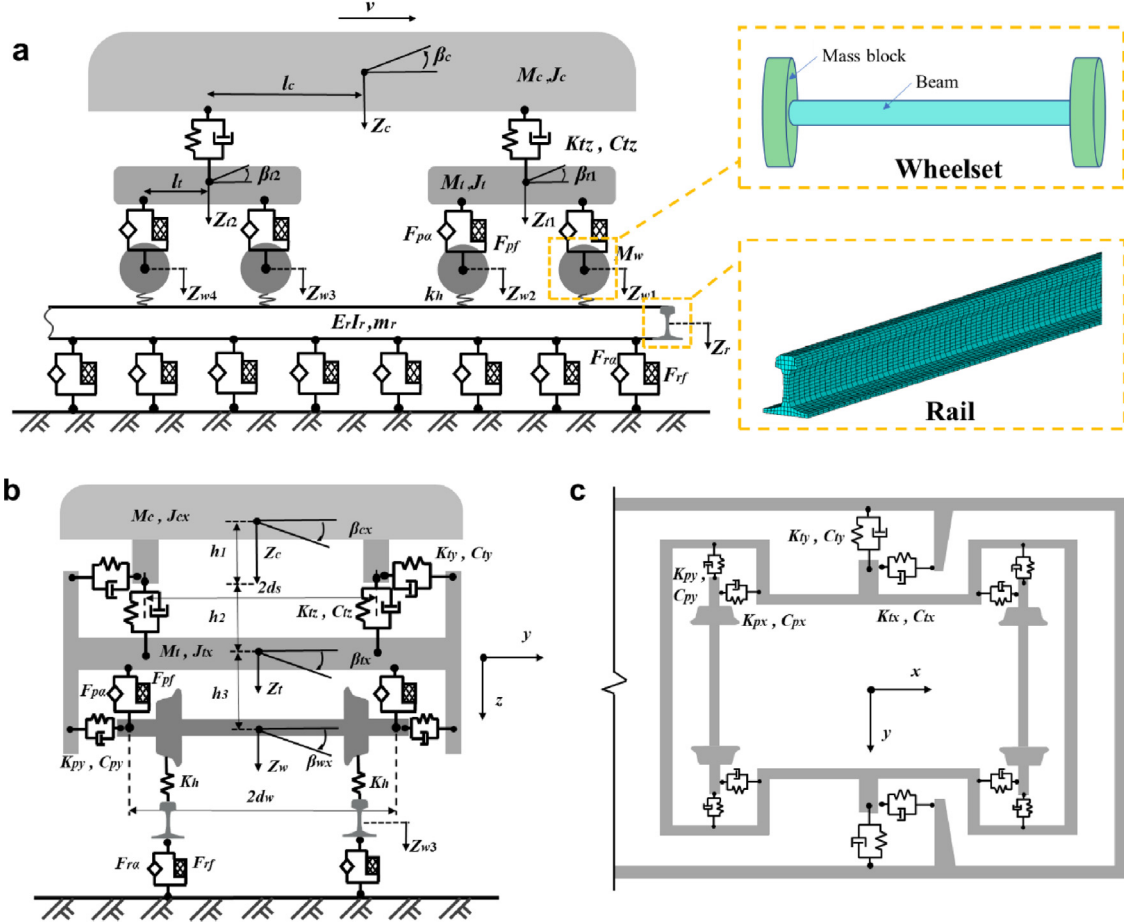


Fig. 2. Side (a), front (b) and top (c) view of nonlinear fractional Zener model of the vehicle system. Top right inset 1: the elastic model of wheelset; Top right inset 2: Solid element rail model.

rear bogie (β_{cy} , β_{ty1} , β_{ty2}); (3) rolling angle of the car body, front bogie and rear bogie (β_{cx} , β_{tx1} , β_{tx2}).

The wheelsets are modeled by the elastic model combining the beam and mass block, as shown in Fig. 2a. In this elastic model, the wheel axle is simulated by Timoshenko beam, while the wheel is modeled by a rigid mass block. By utilizing the proposed flexible wheelset model, the dynamic response of the vehicle system in the high-frequency domain can be more accurately obtained than the classic rigid wheelset model.

To better understand and deduce the dynamic equations of the vehicle and track, Fig. 3 gives a schematic sketch of the serial number of the primary suspensions and rails at both ends of the wheelsets. The lower (right) and the upper (left) rails are numbered as No. 1 and No. 2, respectively. The numbers (1~8) of the primary suspensions are also shown in the figure, and the numbers of wheel locations are the same

as the suspension numbers. The dynamic response of each part in the vehicle system can be described as follows.

(1) The linear dynamic equations of the car body can be written as follows [46].

$$M_c \ddot{Z}_c + 2C_{tz} \dot{Z}_c - C_{tz} (\dot{Z}_{t1} + \dot{Z}_{t2}) + 2K_{tz} Z_c - K_{tz} (Z_{t1} + Z_{t2}) = M_c g \quad (4)$$

$$J_{cy} \ddot{\beta}_{cy} + 2(C_{tz} l_c^2 + C_{tx} h_1^2) \dot{\beta}_{cy} + 2(K_{tz} l_c^2 + K_{tx} h_1^2) \beta_{cy} + C_{tz} l_c (\dot{Z}_{t1} - \dot{Z}_{t2}) + K_{tz} l_c (Z_{t1} - Z_{t2}) + C_{tx} h_1 h_2 (\dot{\beta}_{ty1} + \dot{\beta}_{ty2}) + K_{tx} h_1 h_2 (\beta_{ty1} + \beta_{ty2}) = 0 \quad (5)$$

$$J_{cx} \ddot{\beta}_{cx} + 2(C_{ty} h_1^2 + C_{tz} d_s^2) \dot{\beta}_{cx} + 2(K_{ty} h_1^2 + K_{tz} d_s^2) \beta_{cx} + (C_{ty} h_1 h_2 - C_{tz} d_s^2) (\dot{\beta}_{tx1} + \dot{\beta}_{tx2}) + (K_{ty} h_1 h_2 - K_{tz} d_s^2) (\beta_{tx1} + \beta_{tx2}) = 0 \quad (6)$$



Fig. 3. Schematic drawing of the serial number of primary suspensions.

where, M_c , K_{ly} , K_{tz} , C_{ly} , C_{tz} represent the car body mass, the lateral and vertical stiffness, and damping matrices of the secondary suspension; J_{cy} , J_{cx} are the moment of inertia around the y -axis and x -axis, respectively; l_c is the half of the bogie spacing; h_1 is the distance between the car body center and upper surface of secondary suspension; h_2 is distance between bogie frame center and upper surface of secondary suspension; d_s is secondary suspension lateral span.

(2) The nonlinear dynamic equations of the first bogie can be expressed as follows [46].

$$M_t \ddot{Z}_t + C_{tz} \dot{Z}_t - C_{tz} \dot{Z}_{t1} + C_{tz} l_c \dot{\beta}_{cy} + K_{tz} Z_t - K_{tz} Z_{t1} + K_{tz} l_c \beta_{cy} - F_{pa1} - F_{pa2} - F_{pa5} - F_{pa6} - F_{pf1} - F_{pf2} - F_{pf5} - F_{pf6} = M_t g \quad (7)$$

$$J_{ty} \ddot{\beta}_{ty1} + 2(C_{px} h_3^2 + C_{tx} h_2^2) \dot{\beta}_{ty1} + 2(K_{px} h_3^2 + K_{tx} h_2^2) \beta_{ty1} + (F_{pa1} - F_{pa2} + F_{pa5} - F_{pa6}) l_t + (F_{pf1} - F_{pf2} + F_{pf5} - F_{pf6}) l_t + C_{tx} h_1 h_2 \dot{\beta}_{cy} + K_{tx} h_1 h_2 \beta_{cy} = 0 \quad (8)$$

$$J_{tx} \ddot{\beta}_{tx1} + 2(C_{ty} h_2^2 + C_{tz} d_s^2 + C_{py} h_3^2) \dot{\beta}_{tx1} + 2(K_{ty} h_2^2 + K_{tz} d_s^2 + K_{py} h_3^2) \beta_{tx1} + (C_{ty} h_1 h_2 - C_{tz} d_s^2) \dot{\beta}_{cx} + (K_{ty} h_1 h_2 - K_{tz} d_s^2) \beta_{cx} + (F_{pa5} + F_{pa6} - F_{pa1} - F_{pa2}) d_w + (F_{pf5} + F_{pf6} - F_{pf1} - F_{pf2}) d_w = 0 \quad (9)$$

The equation of motion of the second bogie can be obtained in the same manner. Where, M_t is bogie mass matrix; F_{ta1} , F_{tf1} are the FD viscous force and nonlinear friction force of the primary suspensions, respectively; J_{ty} , J_{tx} is the moment of inertia around y -axis and x -axis, respectively; l_t is half of the wheelset spacing; d_w is the primary suspension lateral span; h_3 is the distance between the bogie frame center and lower surface of the primary suspension.

(3) The nonlinear dynamic equation of vertical displacement Z_{w1} of the first wheelset is given as follows [46].

$$M_w(x) \frac{\partial^2 Z_{w1}(x, t)}{\partial t^2} + K_{w1} Z_{w1}(x, t) = -F_{pa1} - F_{pf1} - p_1(t) - F_{pa5} - F_{pf5} - p_5(t) + M_w(x) g \quad (10)$$

In this paper, the wheelset is treated as a beam and mass block model instead of the rigid body model. In Eq. (9), $M_w(x)$ is the mass distribution function of the wheelset, $Z_{w1}(x, t)$ is the vertical displacement of the first wheelset, K_{w1} is the system stiffness of the elastic model of the first wheelset; $p_1(t)$ is the wheel-rail force located at the first wheel-rail contact point.

The normalized modal function of the elastic model of wheelset is defined as the matrix Φ_{wz} , which can be expressed as following [47].

$$\Phi_{wz} = \left(\begin{array}{c} \left\{ \begin{array}{c} x_1 \\ x_2 \\ x_3 \\ \vdots \\ x_{M_1} \end{array} \right\}, \left\{ \begin{array}{c} x_1 \\ x_2 \\ x_3 \\ \vdots \\ x_{M_1} \end{array} \right\}, \left\{ \begin{array}{c} x_1 \\ x_2 \\ x_3 \\ \vdots \\ x_{M_1} \end{array} \right\}, \dots, \left\{ \begin{array}{c} x_1 \\ x_2 \\ x_3 \\ \vdots \\ x_{M_1} \end{array} \right\} \end{array} \right)_{M_1 \times N_1} \quad (11)$$

where, $\varphi_{wzi}(x_i)$ represents the modal deformation value of the i th vertical characteristic mode of the elastic model at the coordinate x_i , M_2 is the total number of nodes of the elastic wheelset model, N_1 is the total order of the modes.

Therefore, the solution of the equation of motion of the i th wheelset can be written in the modal space as follows [47].

$$Z_{wi}(x, t) = -\Phi_{wz} q_{wi}(t) \quad (12)$$

where, $q_{wi}(t)$ is the coordinate of the displacement response of the i th wheelset in the modal space, which can be expressed as follows [46].

$$q_{wi}(t) = (q_{wi1}(t), q_{wi2}(t), q_{wi3}(t), \dots, q_{wiN_1}(t))^T \quad (13)$$

In addition, Ω_w can be used to represent the characteristic circle frequency of the elastic model,

$$\Omega_w = (2\pi f_{w1}, 2\pi f_{w2}, 2\pi f_{w3}, \dots, 2\pi f_{wN_1})^T \quad (14)$$

where, f_{wi} is the characteristic frequency corresponding to the i th mode.

Substituting Eq. (11) into Eq. (9), we can get equation as follows.

$$M_w(x_i) \Phi_{wz} \ddot{q}_{w1}(t) + K_{w1} \Phi_{wz} q_{w1}(t) = -F_{pa1} - F_{pf1} - p_1(t) - F_{pa5} - F_{pf5} - p_5(t) + M_w(x_i) g \quad (15)$$

Considering the orthogonality of the modes, Eq. (14) left-multiplied with Φ_{wz}^T can be further rewritten as follows.

$$\ddot{q}_{w1}(t) + (\text{Diag}(\Omega_w))^2 q_{w1}(t) = -\Phi_{wz}(m, :)^T (F_{pa1} + F_{pf1}) - \Phi_{wz}(n, :)^T (F_{pa5} + F_{pf5}) - \Phi_{wz}(j, :)^T p_1(t) - \Phi_{wz}(k, :)^T p_5(t) + \Phi_{wz}^T M_w(x_i) g \quad (16)$$

where, $\text{Diag}(\Omega_w)$ represents the diagonal matrix with the element Ω_w , m and n are the numbers of the nodes at both ends of the elastic wheelset model which connect to the primary suspension, j and k represent the numbers of the nodes of the elastic wheelset model connecting to the two side wheels. The motion equations of the other three wheelsets can be obtained in a similar manner. $\Phi_{wz}(m, :)$ means get the m th row of the matrix Φ_{wz} .

Therefore, the dynamic equation of the vehicle system can be described as follows [46].

$$M_v \ddot{Z}_v(t) + C_v \dot{Z}_v(t) + K_v Z_v(t) = F_v(t) \quad (17)$$

where, M_v , K_v , C_v indicate the generalized mass, stiffness and damping matrices; $Z_v(t)$ is the generalized displacement vectors; F_v is the generalized load vector.

2.2.2. The nonlinear dynamic equation of track structure

The ballastless track system with embedded sleepers consists of rails, fastener systems, slabs, concrete bases and subgrades. Assuming that the track system is symmetrical with respect to its center line, the elastic model of the rail, which is discretely supported on railpads, is established with solid element, as shown in Fig. 2. The coupling relationship between the wheel and rail is based on Hertz contact theory where the elastic half-space assumption holds [48]. Subsequently, the nonlinear FD Zener model of the CVTS is derived by utilizing the

vehicle-track coupling dynamics, FD method, Berg's friction model, and FEM. In the FE model, the rail is modeled by a large number of solid elements, and the accuracy of the track vibration response in high frequency range can be controlled by adjusting the element size [49] and the total order of the track modes employed in the analysis.

In prior research, the beam model of the rail was often simplified by using discrete point supports at sleepers. However, a more realistic approach for the solid element model of the rail is to use a surface-support model that simulates the actual working state of the rail [50,51]. The number of nodes of the rail model on the support surface can be set to N_{face} . Therefore, the nonlinear dynamic equation of the elastic track model can be written as follows.

$$M_r \frac{\partial^2 Z_{rR}(N_f, t)}{\partial t^2} + K_r Z_{rR}(N_f, t) = - \sum_{i=1}^{N_r \times N_{face}} (F_{raRi} + F_{rfRi}) \times \delta(N_f - N_{ri}) + \sum_{j=1}^{N_{wr}} p_j(t) \delta(N_f - N_{wrj}) \quad (18)$$

where, $Z_{rR}(N_f, t)$ represents the displacement of the number N_f node of the No. 1 rail, N_r is the total number of the railpads, N_{ri} is the number i node of the FE model of the rail, N_{wrj} is the number of wheel-rail contact points of the No. 1 rail, which ranges from 1 to 4. M_r and K_r are the mass and stiffness matrices of the rail in the solid element model.

The dynamic equation of the rail can be further efficiently processed and solved by the modal superposition method by considerably reducing the DOFs [46]. The normalized mode functions and corresponding natural frequencies of the elastic model can be conducted with commercial FE software. The normalized mode functions of the elastic model of the rail is defined as Φ_{rz} [52].

$$\Phi_{rz} = \left(\begin{array}{c} \left\{ \begin{array}{c} N_{f1} \\ N_{f2} \\ N_{f3} \\ \vdots \\ N_{fM_2} \end{array} \right\} \\ \left\{ \begin{array}{c} N_{f1} \\ N_{f2} \\ N_{f3} \\ \vdots \\ N_{fM_2} \end{array} \right\} \\ \left\{ \begin{array}{c} N_{f1} \\ N_{f2} \\ N_{f3} \\ \vdots \\ N_{fM_2} \end{array} \right\} \\ \vdots \\ \left\{ \begin{array}{c} N_{f1} \\ N_{f2} \\ N_{f3} \\ \vdots \\ N_{fM_2} \end{array} \right\} \end{array} \right)_{M_2 \times N_2} \quad (19)$$

where, M_2 is the total number of nodes of the elastic rail model, and N_2 is the total order of the rail mode functions, $\Phi_{rzi}(N_{f1})$ represents the vertical displacement of the number N_{f1} node of the i th mode functions.

Therefore, the displacement of the No. 1 rail can be expressed as the form in the modal space as follows [52].

$$Z_{rR}(N_f, t) = \Phi_{rz} q_{rR}(t) \quad (20)$$

where, $q_{rR}(t)$ is the generalized coordinate of the No. 1 rail on the right side, which can be expressed as follows.

$$q_{rR}(t) = \left(q_{rR1}(t), q_{rR2}(t), q_{rR3}(t), \dots, q_{rRN_1}(t) \right)^T \quad (21)$$

Besides, Ω_r can be used to represent the characteristic circle frequency of the solid element model of the rail as follows.

$$\Omega_r = \left(2\pi f_{r1}, 2\pi f_{r2}, 2\pi f_{r3}, \dots, 2\pi f_{rN_1} \right)^T \quad (22)$$

where, f_{ri} is the characteristic frequency of the i th mode of the rail.

Substituting Eq. (19) into Eq. (17), the new equation can be rewritten as follows.

$$M_r \Phi_{rz} \ddot{q}_{rR}(t) + K_r \Phi_{rz} q_{rR}(t) = - \sum_{i=1}^{N_{face}} (F_{raRi} + F_{rfRi}) \delta(N_f - N_{ri}) + \sum_{j=1}^{N_{wr}} p_j(t) \delta(N_f - N_{wrj}) \quad (23)$$

Due to the orthogonality of the mode functions, Eq. (22) can be further rewritten after left-multiplying Φ_{rz}^T as follows.

$$\ddot{q}_{rR}(t) + (\text{Diag}(\Omega_r))^2 q_{rR}(t) = -\Phi_{rz,face}^T (1 : N_{face}, :)^T (F_{raR}(t) + F_{rfR}(t)) + \Phi_{rz,wr}^T (1 : N_{wr}, :)^T p_R(t) \quad (24)$$

where, $\Phi_{rz,face}$ is the vertical displacement of the nodes of the rail mode functions on the rail-railpad contact area; similarly, $\Phi_{rz,wr}$ is the vertical displacement of the nodes of the rail mode functions on the wheel-rail contact area. It is important to note that the nodes of the rail modal function Φ_{rz} can be reduced when the research concern is the vibration characteristics of partial nodes, and then the computation efficiency can be further improved to varying degrees. $\Phi_{rz,face}^T (1 : N_{face}, :)^T$ means the transpose of the rows range from 1 to N_{face} of $\Phi_{rz,face}$.

$$F_{raR} = \left\{ \begin{array}{c} F_{raR1} \\ F_{raR2} \\ F_{raR3} \\ \vdots \\ F_{raRN_{face}} \end{array} \right\}_{N_{face} \times 1}; F_{rfR} = \left\{ \begin{array}{c} F_{rfR1} \\ F_{rfR2} \\ F_{rfR3} \\ \vdots \\ F_{rfRN_{face}} \end{array} \right\}_{N_{face} \times 1}; p_R(t) = \left\{ \begin{array}{c} p_1(t) \\ p_2(t) \\ p_3(t) \\ p_4(t) \end{array} \right\} \quad (25)$$

In the same manner, the dynamic equation of the No. 2 rail on the left side can be obtained.

Since the nonlinear wheel-rail contact model is difficult to be applied for the steady state vibration analysis of the CVTS, the wheel-rail relationship was calculated as the linearized Hertzian contact model [42].

2.3. The steady state vibration response of the CVTS

2.3.1. The equation of motion of the vehicle in frequency domain

Under the harmonic excitation $p_j e^{i\omega t}$, the steady state dynamic response of the vehicle can be expressed as follows [46].

$$\omega^2 M_v Z_v(\omega) + i\omega C_v Z_v(\omega) + K_v Z_v(\omega) = F_v(\omega) \quad (26)$$

The FD Zener model of the No. 1 primary suspension at frequency ω_k can be expressed as follows [53].

$$F_{ta1}(\omega_k) = \frac{k_{ta} + c_{ta}(i\omega_k)^\alpha}{1 + a_{ta}(i\omega_k)^\alpha} (Z_{w1}(\omega_k) - Z_{t1}(\omega_k) + l_t \beta_{ty1}(\omega_k) - d_w \beta_{tx1}(\omega_k)) = (K_{ta}(\omega_k) + i\omega C_{ta}(\omega_k)) (Z_{w1}(\omega_k) - Z_{t1}(\omega_k) + l_t \beta_{ty1}(\omega_k) - d_w \beta_{tx1}(\omega_k)) \quad (27)$$

where, α , k_{ta} , c_{ta} , a_{ta} are the FD Zener model coefficients of the primary suspension, C_{ta} and K_{ta} represent the corresponding equivalent frequency-dependent damping and stiffness of the FD Zener model, respectively.

By employing the simplified Berg's friction schemes, the friction $F_{tf}(\omega)$ of the No. 1 primary suspensions in the frequency domain can be described as follows [42].

$$F_{tf1}(\omega_k) = (K_{tf}(\omega_{k-1}) + i\omega C_{tf}(\omega_{k-1})) (Z_{w1}(\omega_k) - Z_{t1}(\omega_k) + l_t \beta_{ty1}(\omega_k) - d_w \beta_{tx1}(\omega_k)) \quad (28)$$

The FD Zener model and the simplified friction model of the No. 2~8 primary suspensions can be obtained in the same manner.

2.3.2. The equation of motion of the track structure in the frequency domain

Under the harmonic excitation $p_R e^{i\omega t}$, the dynamic equation of the elastic track structure modeled with FEM can be expressed as follows.

$$\omega^2 q_{rR}(\omega) + (\text{Diag}(\Omega_r))^2 q_{rR}(\omega) = -\Phi_{rz,face}^T (1 : N_{face}, :)^T (F_{raR}(\omega) + F_{rfR}(\omega)) + \Phi_{rz,wr}^T (1 : N_{wr}, :)^T p_R(\omega)$$

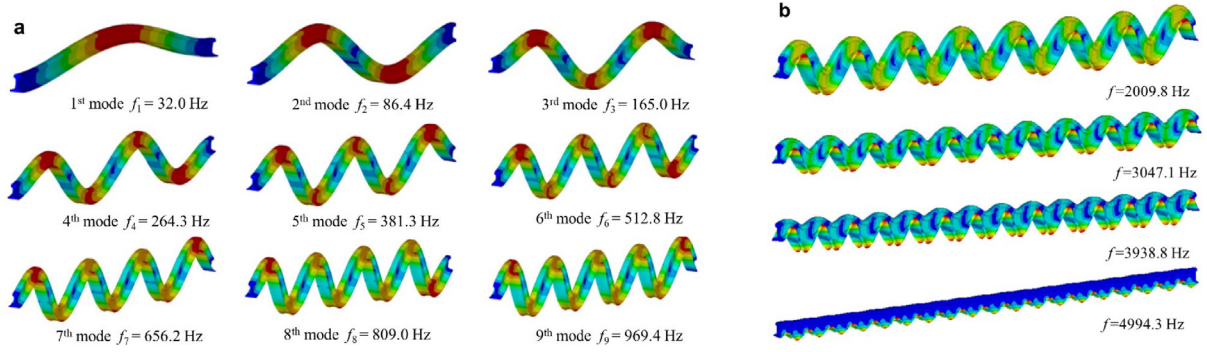


Fig. 4. Vertical modes of the solid element rail model. (a) The first nine modes; (b) the modes near 2~5 kHz.

$$+ F_{rfR}(\omega) + \Phi_{rz,wr}(1:N_{wr}, :)^T p_R(\omega) \quad (29)$$

where, $p_R(\omega)$ is the wheel–rail force of the No. 1 rail in the frequency domain, and it can be expressed as follows.

$$p_R(\omega) = \begin{Bmatrix} p_1(\omega) \\ p_2(\omega) \\ p_3(\omega) \\ p_4(\omega) \end{Bmatrix} \quad (30)$$

The fractional railpad force $F_{raRi}(\omega)$ of the FD Zener model on each node belongs to the rail–railpad contact area can be expressed as follows.

$$F_{raRi}(\omega_k) = \frac{k_r + c_{ra}(i\omega_k)^\alpha}{1 + a_{ra}(i\omega_k)^\alpha} Z_{rR}(N_{ri}, \omega_k) / N_{face} \\ = (K_{ra} + i\omega_k C_{ra}) Z_{rR}(N_{ri}, \omega_k) / N_{face} \quad (31)$$

where, k_{ra} , c_{ra} , α , a_{ra} are the FD Zener model coefficients of the railpad, C_{ra} and K_{ra} indicate the corresponding equivalent frequency-dependent damping and stiffness of the railpad, respectively.

According to the simplified Berg's friction force model, similarly, the friction force $F_{rfRi}(\omega)$ on each node belongs to the rail–railpad contact area can be expressed as follows [42].

$$F_{rfRi}(\omega_k) = (K_{rf} + i\omega_k C_{rf}) Z_{rR}(N_{ri}, \omega_k) / N_{face} \quad (32)$$

where,

$$Z_{rR}(1:N_{rface}, \omega_k) = \Phi_{rz,face}(1:N_{rface}, :) q_{rR}(\omega_k) \quad (33)$$

The fractional force $F_{raRi}(\omega)$ and friction force $F_{rfRi}(\omega)$ of the railpad force can be further rewritten as follows in the modal space.

$$F_{raRi}(\omega_k) = (K_{ra} + i\omega_k C_{ra}) \Phi_{rz,face}(1:N_{rface}, :) \ddot{q}_{rR}(\omega_k) / N_{face} \quad (34)$$

$$F_{rfRi}(\omega_k) = (K_{rf} + i\omega_k C_{rf}) \Phi_{rz,face}(1:N_{rface}, :) \ddot{q}_{rR}(\omega_k) / N_{face} \quad (35)$$

The displacement response of the j th wheelset at the wheel–rail contact point in the frequency domain can be expressed as follows.

$$Z_{wj}(\omega_k) = \Phi_{wz}(k, :) q_{wj}(\omega_k) \quad (36)$$

The right rail at the wheel–rail contact points can be expressed as follows.

$$Z_{rR}(N_{wrj}, \omega_k) = \Phi_{rz,wr}(1:4, :) q_{rR}(\omega_k) \quad (37)$$

where,

$$\Phi_{rz,wr}(1:4, :) = \begin{Bmatrix} \Phi_{rz}(N_{wr1}, :) \\ \Phi_{rz}(N_{wr2}, :) \\ \Phi_{rz}(N_{wr3}, :) \\ \Phi_{rz}(N_{wr4}, :) \end{Bmatrix} \quad (38)$$

Hence, the dynamic equation of the right rail in the modal coordinates can be obtained,

$$\omega^2 q_{rR}(\omega) + (\text{Diag}(\Omega r))^2 q_{rR}(\omega) = -\Phi_{rz,face}(1:N_{rface}, :)^T \\ \times (K_{ra} + i\omega_k C_{ra} + K_{rf} + i\omega_k C_{rf}) \Phi_{rz,face}(1:N_{rface}, :) \\ \times q_{rR}(\omega) / N_{face} + \Phi_{rz,wr}(1:N_{wr}, :)^T k_h(\Phi_{wz}(k, :) q_w(\omega_k) \\ - \Phi_{rz,wr}(1:N_{wr}, :) q_{rR}(\omega_k) - r_R(\omega_k)) \quad (39)$$

The dynamic equation of the left rail can be obtained in the same manner.

3. Results and discussion

In this section, we first compare the natural vibration characteristics of the rail with the beam model and FEM (Section 3.1), and then analyze the effects of the FE rail model, elastic wheelset and surface-supported railpad configuration on the dynamic behavior of the CVTS (Section 3.2).

3.1. Natural vibration characteristics of the rail in two different models

The modal superposition method was employed to improve the calculation efficiency of the proposed refined FDZ model of the CVTS by considerably reducing the degrees of freedoms of the rail [52]. The natural modes of the rail modeled by the Solid 45 can be efficiently and accurately solved by ANSYS FE software using Block Lanczos method. Besides, the modal analysis of the rail with the Timoshenko beam model was also conducted to compare their different vibration characteristics. The model length of the rail was set as 3 m, and the boundary condition was considered as fixed constraints on each end face. The element size in the FE model was selected as 0.03 m through converging analysis, and the first 500 vibration modes were extracted. Fig. 4 presents representative vertical mode shapes and their corresponding characteristic frequencies within the range of 5000 Hz.

Fig. 4a shows the first nine mode shapes and their corresponding natural frequencies of the modes by solid element rail model. These mode shapes in the low frequency range are close to the theoretical sine functions, and hence the Timoshenko beam model can have acceptable accuracy to the solid element model while using the Ritz mode. However, the vertical mode deformations of the solid element model near 2~5 kHz show significant differences between the rail head and rail foot (see Fig. 4b), which contrasts with the beam model's assumption that the mode displacements on the rail's cross-section are uniform. The differences between these two models thus become significant in the high frequency domain.

According to the modal analysis of the rail, it can be found that the solid element model reveals more detailed deformation characteristics in the high frequency range in comparison to the beam model, so the random vibration analysis of the rail can be simulated more accurately and comprehensively. The natural vibration characteristics

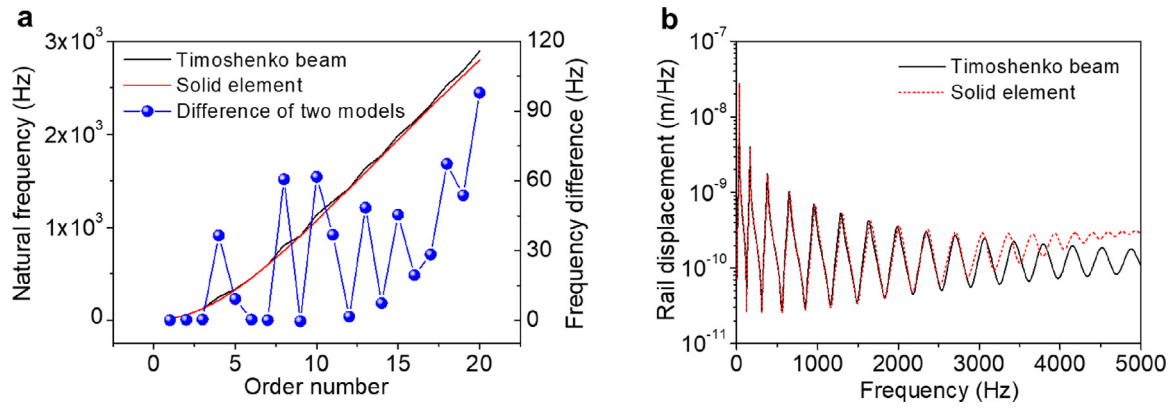


Fig. 5. Comparison for the rail dynamic characteristics of the Timoshenko beam model and solid element model. (a) natural frequency; (b) harmonic response.

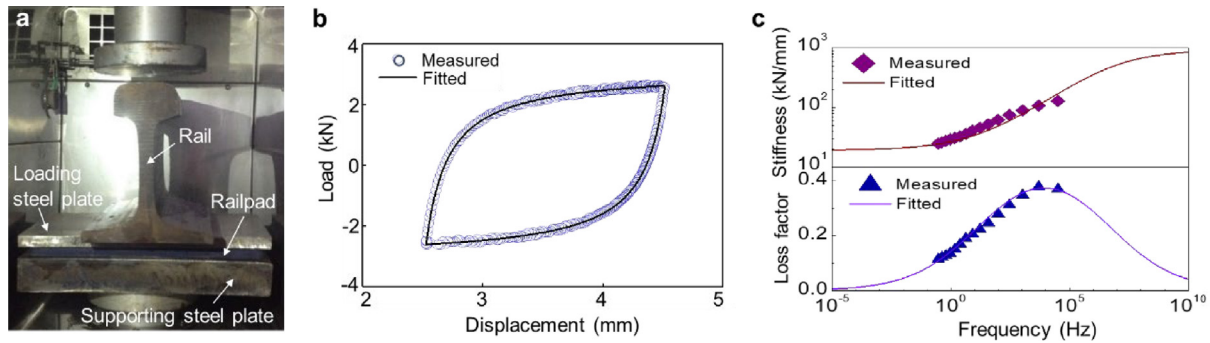


Fig. 6. (a) The test setup of the full-size railpad in Vossloh 300 fasteners; (b) the force-displacement hysteresis curve of experiment results; (c) the measured and fitted data of the storage stiffness and loss factor under different frequencies.

of the rail between the solid element model and the Timoshenko beam model were further investigated, as shown in Fig. 5. Fig. 5a compares the natural frequencies of the rail in the two models. The analysis indicates that, except for the fourth and eighth modes, the natural frequency differences between the two models can be neglected within 1 kHz. Nevertheless, the differences become more pronounced when the frequency exceeds 1 kHz, demonstrating the superior simulation accuracy of the solid element model with accurate representation of rail cross-section deformation.

To further compare the vibration characteristics of the two rail models, a fixed beam model of the rail with a length of 6 m and a damping ratio of 0.02 was analyzed through harmonic response analysis. The model's response to a unit load applied at the midspan was obtained, as shown in Fig. 5b. While the harmonic responses of the two models show negligible differences in the 2 kHz range, the disparity increases gradually over 2 kHz. Throughout the frequency domain, the displacement of the solid element model is slightly higher than that of the beam model, while the solid element model's dominant frequencies are lower than those of the beam model. This discrepancy becomes more significant in the higher frequency range, primarily due to the solid element model's lower bending stiffness compared to the stiffer beam model [54].

3.2. Analysis of the refined nonlinear FD Zener model of the CVTS

The simulation scenario of vehicle-track coupled dynamics was considered as a railway vehicle traveling at a speed of 300 km/h, and the German high-speed irregularity spectrum was implemented as the input excitation with a wavelength range of 0.02~200 m. The nonlinear FD Zener model parameters of railpads and the primary suspension are present in Section 3.2.1, and the random vibration analysis of CVTS is given in Section 3.2.2.

Table 1

FD Zener model coefficients of the railpad.

Item	a_{ra} (s ^{-α})	b_{ra} (N/m)	c_{ra} (N s ^{-α} /m)	α
Value	5.6e-3	1.96e7	5.2e6	0.3

3.2.1. Nonlinear FD zener model parameters of railpads and the primary suspension

The parameters of the railpad used in Vossloh 300 fasteners are obtained by laboratory experiments [42]. The mechanical properties of the railpad were measured in a temperature range of -60 °C to 20 °C using a full-size railpad test setup, as shown in Fig. 6a. The dynamic response of the railpad was evaluated by measuring the hysteresis force-displacement curve, as shown in Fig. 6b. Berg's friction model was used to fit the nonlinear coefficients of the railpad, which were determined as $F_{fmax} = 4.1$ kN and $x_2 = 0.1$ mm. The frequency-dependent dynamic coefficients of the railpad were obtained using the Williams-Landel-Ferry equation and the Time-Temperature Superposition principle, as shown in Fig. 6c, based on experimental data at different temperature points. The coefficients in the FD Zener model were determined based on the obtained frequency-dependent dynamic coefficients, and are presented in Table 1. These nonlinear parameters of the railpads were utilized for subsequent modeling and simulation analyses. The nonlinear parameters of the primary suspension were obtained from the literature [38].

3.2.2. Comparison analysis of the frequency response of the CVTS

Fig. 7 shows the acceleration responses of the bogie, wheelset, rail and wheel-rail force in the frequency domain under the two different rail models. The effect of the rail models on the bogie acceleration response is negligible within 200 Hz, since the dynamic response of the CVTS is primarily affected by the rail models in the high frequency

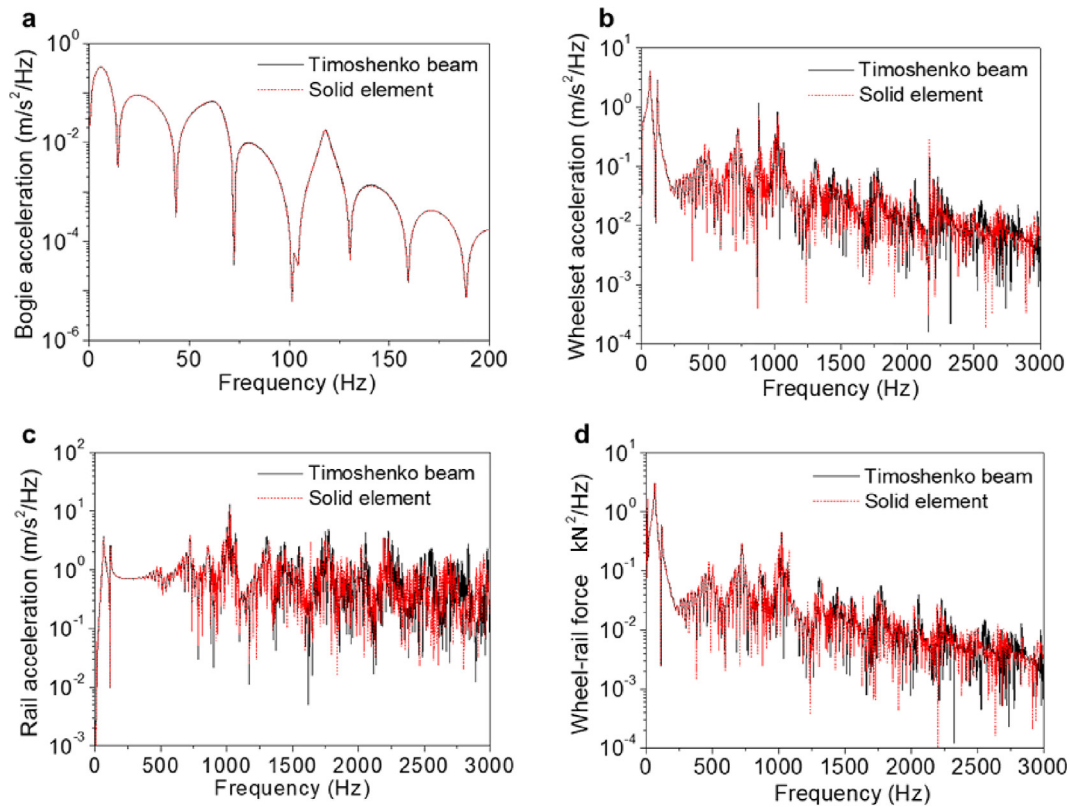


Fig. 7. Acceleration of the CVTS in two different rail models. (a) Bogie; (b) Wheelset; (c) Rail; (d) Wheel-rail force.

domain, as shown in Fig. 7a. It can be observed that the dynamic response of the wheelset and rail acceleration, and wheel-rail force have a similar variation trend within 3 kHz, and the accuracy difference between the two rail models is relatively small in the range of 0~1 kHz (see Fig. 7b~d). Specifically, for wheel-rail force, the difference in response peak at the first dominant frequency of 64.3 Hz is only 0.8%, while that near the dominant frequency of 723 Hz is about 3%. However, the differences between the two models gradually increase in the range of 0~1 kHz, becoming significant over 2 kHz. Based on this comparison analysis, it can be concluded that the nonlinear FD Zener model of the CVTS, which employs the Timoshenko beam model of rail, can achieve relatively accurate response results within 1 kHz, but its accuracy cannot be guaranteed above 1 kHz. Therefore, when studying the random vibration characteristics above 1 kHz, a solid element model should be utilized for the CVTS. Further field experimental validation of this finding is expected to be performed in future research.

he solid element model of the rail in the CVTS offers another notable advantage, which is the ability to obtain the dynamic response of the rail at any spatial coordinate. To investigate the variation in vibration response across different locations on the cross-section of the rail, five representative positions were identified and labeled on the rail cross-section, as shown in Fig. 8a. The numerical labels assigned to these positions (①~⑤) correspond to the five specific locations on the rail, namely, the railhead edge, railhead, rail web, rail foot, and rail foot edge.

Fig. 9a~c present the comparison of the rail acceleration at different local positions. Fig. 9a shows that the rail vibration responses at points 1 and 2 match well in most of the frequency range, except for noticeable differences in the response peaks in the frequency range of 1.05–1.7 kHz. The rail responses at three points 2, 3, and 5, located on

the symmetry axis of the rail cross-section, show slight differences (see Fig. 9b). However, the rail vibration at points 4 and 5 have significant differences throughout frequency domain (see Fig. 9c). The amplitude peaks at point 5 exceed those of point 4 within 1.3 kHz, while the inverse results appear in the frequency range of 1.3–3 kHz. This is due to the rail foot edge's increased susceptibility to deformation under certain frequency excitations, which can also be distinguished by the different deformation of the natural modes in these two local regions, as depicted in Fig. 4.

The random vibration of the CVTS under two models of the wheel axle, namely the elastic model and the rigid model, was investigated. The results depicted in Fig. 9d demonstrate significant differences in the bogie response between the two models for frequencies above 20 Hz. In Fig. 9e, the wheelset response shows a noticeable distinction at the first dominant frequency of approximately 65 Hz, with the elastic model revealing three additional response peaks at 118.4 Hz, 879.4 Hz, and 2166.4 Hz, which are the characteristic modes excited by the symmetric load of the two rails.

Previous studies on the railpad configuration for the CVTS have generally assumed a simple support on a series of single points (see Fig. 8b). However, in reality, the rail is supported on a certain surface by the railpad (see Fig. 8c), which can significantly affect the random vibration of the rail and wheelsets in the high frequency domain. The comparison analysis results in Fig. 9 show that the bogie response under these two railpad configuration models has only a slight difference in the entire frequency domain. At the first dominant frequency of 64.3 Hz, the rail acceleration difference between these two support models is only 0.1% (see Fig. 9f). However, using the simplified railpad model as the single point-support, there is a significant impact on the response in the frequency range of 950 Hz–1150 Hz, and the peak difference at 1 kHz for these two models exceeds 41%. Additionally,

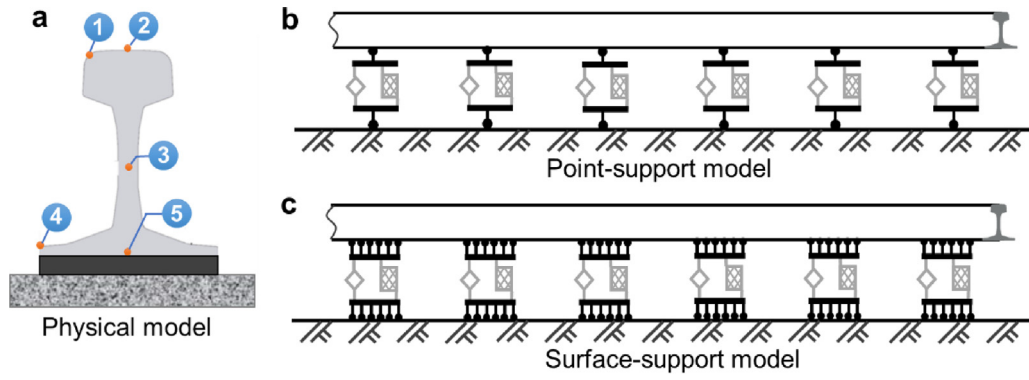


Fig. 8. (a) Number of points at different positions of rail section; (b) point-support and (c) surface-support model of rail.

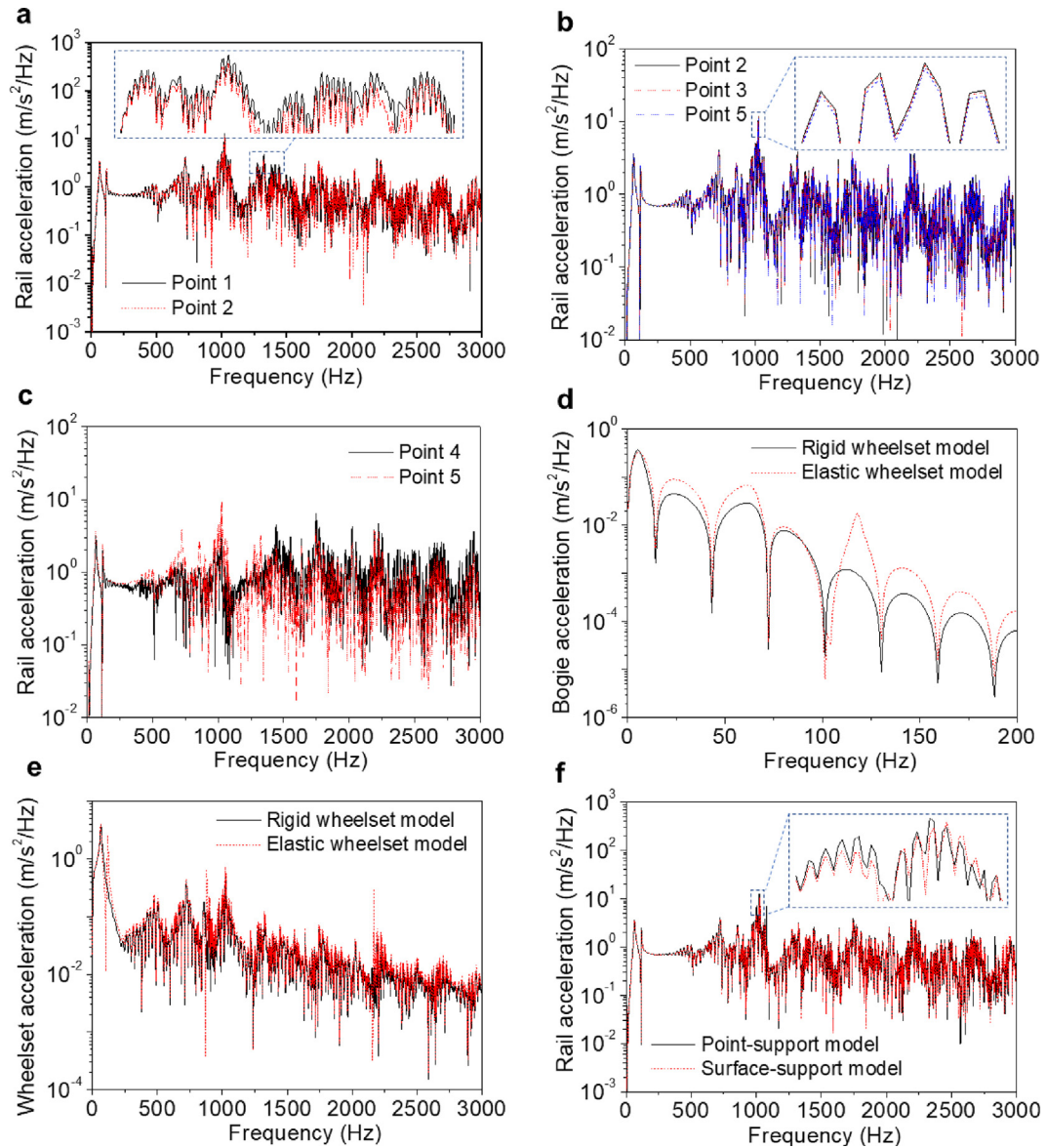


Fig. 9. (a), (b), (c) Comparison of rail acceleration of different points on the rail cross section; (d) Bogie and (e) wheelset acceleration of rigid wheelset model and elastic wheelset model; (f) Rail acceleration of two constraint models of rail.

there is an obvious difference in the response in the frequency range of 2.4 kHz to 3 kHz, with the acceleration difference of the rail near 2650 Hz being greater than 44%. The dynamic responses of the

wheelsets under these two support models exhibit a similar trend to the rail in the entire frequency domain. Therefore, optimizing the support model of the railpad as a surface-support is essential to obtain a more

accurate simulation of the random vibration of the CVTS in the high frequency domain.

Conclusion

By simultaneously employing the nonlinear FD Zener models of the railpads and primary suspension, finite element rail model, elastic wheel axle model, and surface-support railpad configuration, a refined numerical model of the CVTS was developed to better simulate the high frequency dynamics. Combined with the modal superposition method, the proposed model has high calculation accuracy as well as high computation efficiency.

In the high frequency domain, the solid element model shows notable differences in modal deformations between the rail head and foot. Although the bogie response difference between the solid element model and the classic model of the CVTS can be disregarded due to the damping effect of the primary suspension system, the Timoshenko beam model limits to provide accurate results for the wheel-rail force above 1 kHz. The acceleration of different positions on the rail head shows minor differences in most frequency ranges, except for the range of 1.05~1.7 kHz, while the responses of the rail foot and foot edge exhibit conspicuous differences throughout the frequency domain.

In the CVTS, when assuming the wheel axle to be an elastic model, there is an 11% discrepancy in the bogie response at the first dominant frequency, while a noticeable difference in the entire frequency range is observed in the response of the wheelset compared to those of the rigid model. Additionally, to accurately simulate the random vibration of the CVTS in the high-frequency domain, the railpad configuration was modeled as a surface-support model, which resulted in peak differences of more than 41% at 1 kHz and 44% at 2650 Hz in the rail acceleration response, as compared to the point-support model.

This work contributes to a better understanding of the vehicle-track coupled dynamics in the high-frequency range by the comparison analysis of the proposed refined model and the classic model. The refined model more realistically simulate the rail, wheel axle, nonlinear railpads and primary suspension, and hence can better reproduce the high-frequency vehicle-track dynamics. In future research, a thorough validation of the proposed nonlinear model against the field experiments and other published numerical model will be performed to better demonstrate its effectiveness.

CRediT authorship contribution statement

Fan Yang: Conceptualization, Methodology, Formal analysis, Data curation, Investigation, Software, Writing – original draft, Writing – review & editing. **Pan Zhang:** Methodology, Formal analysis, Data curation, Investigation, Writing – original draft, Writing – review & editing. **Yuan Wang:** Methodology, Formal analysis, Data curation, Investigation, Writing – review & editing. **Kai Wei:** Methodology, Investigation, Resources, Writing – review & editing, Supervision, Project administration. **Liwei Dong:** Formal analysis, Data curation, Writing – review & editing. **Ping Wang:** Investigation, Resources, Writing – review & editing, Supervision, Project administration, Funding acquisition.

Declaration of competing interest

The authors declare that they have no known competing financial interests or personal relationships that could have appeared to influence the work reported in this paper.

Data availability

The data that has been used is confidential.

Acknowledgments

This research was supported by the National Outstanding Youth Science Foundation of China (Grant No. 51425804), National Natural Science Foundation of China (Grant No. 12202276 and 51978583), and National Key Research and Development Project (Grand No. 2021YFB3703801-1).

References

- [1] M. Ignesti, A. Innocenti, L. Marini, E. Meli, A. Rindi, P. Toni, Wheel profile optimization on railway vehicles from the wear viewpoint, *Int. J. Non-Linear Mech.* 53 (2013) 41–54.
- [2] H. Wu, P. Wu, F. Li, H. Shi, K. Xu, Fatigue analysis of the gearbox housing in high-speed trains under wheel polygonization using a multibody dynamics algorithm, *Eng. Fail. Anal.* 100 (2019) 351–364.
- [3] X. Cui, X. Ling, Effects of differential subgrade settlement on damage distribution and mechanical properties of CRTS II slab track, *Constr. Build. Mater.* 271 (2021) 121821.
- [4] C. Ma, L. Gao, T. Xin, X. Cai, M.M. Nadakatti, P. Wang, The dynamic resonance under multiple flexible wheelset-rail interactions and its influence on rail corrugation for high-speed railway, *J. Sound Vib.* 498 (2021) 115968.
- [5] Z. Wei, X. Sun, F. Yang, Z. Ke, T. Lu, P. Zhang, C. Shen, Carriage interior noise-based inspection for rail corrugation on high-speed railway track, *Appl. Acoust.* 196 (2022) 108881.
- [6] J. Maes, H. Sol, P. Guillaume, Measurements of the dynamic railpad properties, *J. Sound Vib.* 293 (2006) 557–565.
- [7] M.M. Sjöberg, L. Kari, Non-linear behavior of a rubber isolator system using fractional derivatives, *Veh. Syst. Dyn.* 37 (2002) 217–236.
- [8] M. Sol-Sánchez, F. Moreno-Navarro, M.C. Rubio-Gámez, The use of elastic elements in railway tracks: A state of the art review, *Constr. Build. Mater.* 75 (2015) 293–305.
- [9] B. Blanco, A. Alonso, L. Kari, N. Gil-Negrete, J. Giménez, Implementation of timoshenko element local deflection for vertical track modelling, *Veh. Syst. Dyn.* 57 (2019) 1421–1444.
- [10] S.P. Timoshenko, D.H. Young, W.J. Weaver, *Vibration Problem in Engineering*, 1990.
- [11] K. Koro, K. Abe, M. Ishida, T. Suzuki, Timoshenko beam finite element for vehicle-track vibration analysis and its application to jointed railway track, *Proc. Inst. Mech. Eng. F* 218 (2004) 159–172.
- [12] Z. Yang, P. Zhang, L. Wang, Wheel-rail impact at an insulated rail joint in an embedded rail system, *Eng. Struct.* 246 (2021) 113026.
- [13] P. Zhang, S. Li, Z. Li, Short pitch corrugation mitigation by rail constraint design, *Int. J. Mech. Sci.* (2022) 108037.
- [14] L. Han, L. Jing, L. Zhao, Finite element analysis of the wheel-rail impact behavior induced by a wheel flat for high-speed trains: the influence of strain rate, *Proc. Inst. Mech. Eng. F* 232 (2018) 990–1004.
- [15] B. Wu, Z. Shang, J. Pan, R. Zhang, P. Shi, P. Xiao, Analysis on the formation cause for the high-order wheel polygonization of the high-speed trains based on the finite element method, *Veh. Syst. Dyn.* 61 (2023) 1–18.
- [16] K. Wei, Y. Dou, F. Wang, P. Niu, P. Wang, Z. Luo, High-frequency random vibration analysis of a high-speed vehicle-track system with the frequency-dependent dynamic properties of rail pads using a hybrid SEM-SM method, *Veh. Syst. Dyn.* 56 (2018) 1838–1863.
- [17] K. Wei, Q. Yang, Y. Dou, F. Wang, P. Wang, Experimental investigation into temperature-and frequency-dependent dynamic properties of high-speed rail pads, *Constr. Build. Mater.* 151 (2017) 848–858.
- [18] J. Martínez-Casas, J. Giner-Navarro, L. Baeza, F. Denia, Improved railway wheelset-track interaction model in the high-frequency domain, *J. Comput. Appl. Math.* 309 (2017) 642–653.
- [19] P. Torstensson, J.C. Nielsen, L. Baeza, Dynamic train-track interaction at high vehicle speeds—Modelling of wheelset dynamics and wheel rotation, *J. Sound Vib.* 330 (2011) 5309–5321.
- [20] A. Śladkowski, K. Bizoń, The use of semi-automatic technique of finite elements mesh generation for solutions of some railway transport problems, *Mechanics* 23 (2017) 190–196.
- [21] K. Knothe, Z. Strzykowski, K. Willner, Rail vibrations in the high frequency range, *J. Sound Vib.* 169 (1994) 111–123.
- [22] X. Lei, J. Wang, Dynamic analysis of the train and slab track coupling system with finite elements in a moving frame of reference, *J. Vib. Control* 20 (2014) 1301–1317.
- [23] L. Baeza, J. Giner-Navarro, D.J. Thompson, J. Monterde, Eulerian models of the rotating flexible wheelset for high frequency railway dynamics, *J. Sound Vib.* 449 (2019) 300–314.
- [24] L. Xu, Q. Zhang, Z. Yu, Z. Zhu, Vehicle-track interaction with consideration of rail irregularities at three-dimensional space, *J. Vib. Control* (2020) 1077546319894816.

- [25] K. Liu, L. Jing, A finite element analysis-based study on the dynamic wheel-rail contact behaviour caused by wheel polygonization, *Proc. Inst. Mech. Eng. F* (2019) 0954409719891549.
- [26] X. Cui, G. Chen, H. Yang, Q. Zhang, H. Ouyang, M. Zhu, Effect of the wheel/rail contact angle and the direction of the saturated creep force on rail corrugation, *Wear* 330 (2015) 554–562.
- [27] P. Gullers, L. Andersson, R. Lundén, High-frequency vertical wheel-rail contact forces—Field measurements and influence of track irregularities, *Wear* 265 (2008) 1472–1478.
- [28] K. Adolfsson, M. Enelund, Fractional derivative viscoelasticity at large deformations.pdf, *Nonlinear Dynam.* 33 (2003) 301–321.
- [29] R.L. Bagley, P.J. Torvik, Fractional calculus - a different approach to the analysis of viscoelastically damped structures, *AIAA J.* 21 (1983) 741–748.
- [30] T. Pritz, Analysis of four-parameter fractional derivative model of real solid materials, *J. Sound Vib.* 195 (1996) 103–115.
- [31] T. Pritz, Five-parameter fractional derivative model for polymeric damping materials, *J. Sound Vib.* 265 (2003) 935–952.
- [32] A. Schmidt, L. Gaul, Finite element formulation of viscoelastic constitutive equations using fractional time derivatives, *Nonlinear Dynam.* 29 (2002) 37–55.
- [33] D. Ouis, Combination of a standard viscoelastic model and fractional derivative calculus to the characterization of polymers, *Mater. Res. Innov.* 7 (2016) 42–46.
- [34] M. Berg, A model for rubber springs in the dynamic analysis of rail vehicles, *Proc. Inst. Mech. Eng. F* 211 (1997) 95–108.
- [35] M. Berg, A nonlinear rubber spring model for vehicle dynamics analysis, *Veh. Syst. Dyn.* 29 (1998) 723–728.
- [36] Å. Fenander, Frequency dependent stiffness and damping of railpads, *Proc. Inst. Mech. Eng. F* 211 (1997) 51–62.
- [37] Å. Fenander, A fractional derivative railpad model included in a railway track model, *J. Sound Vib.* 212 (1998) 889–903.
- [38] M. Sjöberg, Rubber isolators-measurements and modelling using fractional derivatives and friction, in: *SAE Technical Paper*, 2000.
- [39] M. Sjöberg, L. Kari, Nonlinear isolator dynamics at finite deformations- an effective hyperelastic- fractional derivative- generalized friction model, *Nonlinear Dynam.* 33 (2003) 323–336.
- [40] S. Zhu, C. Cai, P.D. Spanos, A nonlinear and fractional derivative viscoelastic model for rail pads in the dynamic analysis of coupled vehicle-slab track systems, *J. Sound Vib.* 335 (2015) 304–320.
- [41] D. Zhang, S. Zhu, A fractional derivative model for rubber spring of primary suspension in railway vehicle dynamics, *ASCE-ASME J. Risk Uncertain. Eng. Syst. B* 3 (2017).
- [42] F. Yang, P. Wang, K. Wei, F. Wang, Investigation on nonlinear and fractional derivative zener model of coupled vehicle-track system, *Veh. Syst. Dyn.* (2019) 1–26.
- [43] F. Yang, M. Gao, J. Cong, P. Wang, System dynamics modeling and experimental study of railway track with thermoelectric heater/generator in extreme weather conditions, *J. Clean. Prod.* 249 (2020).
- [44] F. Yang, M. Gao, P. Wang, J. Zuo, J. Cong, Efficient piezoelectric harvester for random broadband vibration of rail, *Energy* 218 (2021) 119559.
- [45] M. Gao, C. Su, J. Cong, F. Yang, Y. Wang, P. Wang, Harvesting thermoelectric energy from railway track, *Energy* 180 (2019) 315–329.
- [46] W. Zhai, X. Sun, A detailed model for investigating vertical interaction between railway vehicle and track, *Veh. Syst. Dyn.* 23 (1994) 603–615.
- [47] L. Baeza, A. Roda, J.C. Nielsen, Railway vehicle/track interaction analysis using a modal substructuring approach, *J. Sound Vib.* 293 (2006) 112–124.
- [48] K. Knothe, A. Groz-Thebing, Short wavelength rail corrugation and non-steady-state contact mechanics, *Veh. Syst. Dyn.* 46 (2008) 49–66.
- [49] P. Zhang, S. Li, A. Núñez, Z. Li, Multimodal dispersive waves in a free rail: Numerical modeling and experimental investigation, *Mech. Syst. Signal Process.* 150 (2021) 107305.
- [50] M. Oregui, Z. Li, R. Dollevoet, An investigation into the modeling of railway fastening, *Int. J. Mech. Sci.* 92 (2015) 1–11.
- [51] P. Zhang, S. Li, A. Núñez, Z. Li, Vibration modes and wave propagation of the rail under fastening constraint, *Mech. Syst. Signal Process.* 160 (2021) 107933.
- [52] O.E. Hansteen, K. Bell, On the accuracy of mode superposition analysis in structural dynamics, *Earthq. Eng. Struct. Dyn.* 7 (1979) 405–411.
- [53] N. Gil-Negrete, J. Vinolas, L. Kari, A nonlinear rubber material model combining fractional order viscoelasticity and amplitude dependent effects, *J. Appl. Mech.* 76 (2009).
- [54] D. Thompson, Wheel-rail noise generation, part III: rail vibration, *J. Sound Vib.* 161 (1993) 421–446.